

# Fast fluorescence dynamics in non-ratiometric calcium indicators

M. Gersbach,<sup>1</sup> D. L. Boiko,<sup>2,\*</sup> C. Niclass,<sup>1</sup> C. Petersen,<sup>1</sup> and E. Charbon<sup>1</sup>

<sup>1</sup>*Ecole Polytechnique Fédérale de Lausanne, Quantum Architecture Group, 1015, Lausanne, Switzerland*

<sup>2</sup>*Centre Suisse d'Electronique et de Microtechnique SA, 2002, Neuchâtel, Switzerland*

\*Corresponding author: [dmitri.boiko@csem.ch](mailto:dmitri.boiko@csem.ch)

Compiled August 13, 2021

The fluorescence decay of high-affinity non-ratiometric Ca<sup>2+</sup> indicator Oregon Green BAPTA-1 (OGB-1) is analyzed with unprecedented temporal resolution in two-photon excitation regime. A triple exponential decay is shown to best fit the fluorescence dynamics of OGB-1. We provide a model for accurate measurements of the free Ca<sup>2+</sup> concentration and dissociation constants of non-ratiometric calcium indicators. © 2021 Optical Society of America

OCIS codes: 170.6280, 160.2540, 260.2510, 170.2520, 300.6280, 180.2520.

Fluorescence Lifetime Imaging Microscopy (FLIM) is used to locally probe the chemical environment of fluorophores, e.g., ion concentration, pH, or oxygen content [1, 2]. To acquire time-resolved fluorescence images, the technique of Time-Correlated Single Photon Counting (TCSPC), in combination with detectors exhibiting single-photon sensitivity [3], is commonly used. This technique enables the measurement of photon time-of-arrival distributions with very high accuracies, independently of instabilities in the excitation beam intensity. So far, temporal resolutions of a few hundred picoseconds were considered sufficient in biomedical FLIM applications.

In this letter, we analyze the fluorescence decay of the high-affinity Ca<sup>2+</sup> indicator Oregon Green BAPTA-1 (OGB-1) under two-photon excitation conditions, using a TCSPC system of measured resolution 79ps based on CMOS Single Photon Avalanche Diode (SPAD) detector technology. Our measurements reveal a triple-exponential decay of OGB-1 fluorescence, which we show enables accurate measurements of Ca<sup>2+</sup> concentration and dissociation constants of non-ratiometric fluorescent probes. We provide a comparison with previously reported data [1,4,5], which were acquired at resolution of 200ps.

The SPAD-based TCSPC system is depicted in Fig.1. Our SPADs [6] are integrated in a 32x32 array and incorporate on-chip high bandwidth I/O circuitry. The active region of a SPAD pixel [Fig.1(b)] consists of a p<sup>+</sup>-n junction operating in the Geiger mode. Due to a small diameter (7 μm), our SPADs show an extremely low dark count rate (<10 Hz at room temperature). The photon detection probability is 25 % at 500 nm wavelength, while the dead time is 25 ns with negligible afterpulsing (< 0.1 %) [6].

Fluorescent molecules are excited in the two-photon regime [7], using a mode-locked Ti:Sapphire laser (MaiTai, Spectra Physics) emitting 100 fs optical pulses at 800 nm wavelength [Fig.1(a)]. The attenuated beam with an average power of 9 mW is focused on a sample using a 20x microscope objective (XLUMPlanFL, Olympus), which also serves to collect the fluorescent emission. Fluorescence from OGB-1 samples treated here (central emission wavelength 520 nm) is directed towards the SPAD by a dichroic beam splitter (DBS) and a filter (E650SP, Chroma Technology) for suppression

of backscattered excitation pulses. Another 20x objective images the emission spot onto the SPAD. The low quantum yield of the two-photon excitation fluorescence results in a count rate at the detector of 10 kHz for 80 MHz repetition rate of excitation pulses. Time discrimination is performed in a "reversed start-stop" configuration by measuring the time intervals from a photo-detection event at the SPAD to emission of a successive laser pulse. For precise timing of photon arrivals, we use a 6 GHz bandwidth oscilloscope (WaveMaster, LeCroy) incorporating a time-to-digital converter and enabling computation of histograms of photon arrivals.

Fig.1(c) shows the Instrument Response Function (IRF) of the entire system at 400 nm wavelength (blue curve). It is recorded by measuring the hyper-Rayleigh scattering of 800 nm wavelength pulses in a solution of colloidal gold particles (G1652, Sigma-Aldrich) [8]. At the incident power of 90 mW, the average count rate of the detector is just 600 Hz. The measured photon arrival time jitter of 79 ps (FWHM) is dominated by the SPADs time-response characteristics. The IRF is only slightly asymmetrical and assumes a Gaussian-curve approximation  $IRF = \exp(-t^2/2\sigma_{IRF}^2)$  (inset, cyan curve).

Fluorescent samples were composed of 2 μl OGB-1 dye (O6806, Molecular probes) and 20 μl Ca:EGTA buffer solutions from the calibration kit (C3008MP, Molecular Probes) with quoted free Ca<sup>2+</sup> concentrations in the range of 17 nM to 39 μM. Several fluorescence decay curves measured in the two-photon excitation regime are shown in Fig.1(c). The fluorescence lifetimes were obtained from the numerical analysis of these data.

Thorough numerical fit must take into account the IRF of the system [5]. As opposed to conventional systems with strongly asymmetric IRF, the Gaussian-like IRF of our system assumes a simple analytical expression for the measured fluorescence decay. For a train of excitation pulses of period  $T$ , each term of a multi-exponential decay process reads

$$I_k = \frac{1}{2} \left[ \frac{1 + e^{-T/\tau_k}}{1 - e^{-T/\tau_k}} - \operatorname{erf} \left( \frac{\sigma_{IRF}}{\sqrt{2}\tau_k} - \frac{t}{\sqrt{2}\sigma_{IRF}} \right) \right] \times \exp \left( -\frac{t}{\tau_k} + \frac{\sigma_{IRF}^2}{2\tau_k^2} \right), \quad k = \{f, i, s\} \quad (1)$$

where a triple-exponential decay is assumed and index  $k$  in-

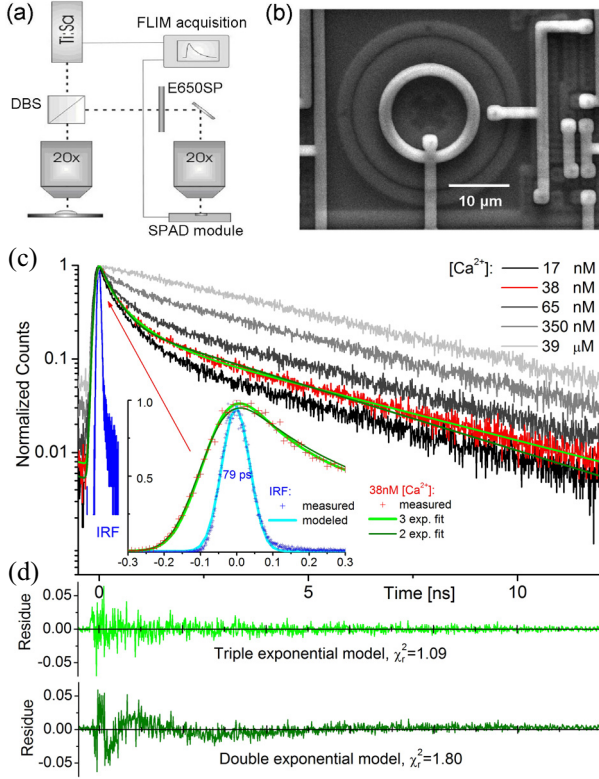


Fig. 1. (Color online) (a) Schematic of the experimental setup for fluorescence lifetime measurements. (b) Scanning electron microscope image of a SPAD. (c) Measured fluorescence decay of OGB-1 at various calcium concentrations (gray scale curves) and hyper-Rayleigh scattering from colloidal gold particles (blue curve). The red curve highlights measured fluorescence decay in a 38 nM free  $\text{Ca}^{2+}$  concentration buffer and the numerical fits of the double-exponential (olive curve,  $\chi_r^2=1.80$ ) and triple-exponential (green curve,  $\chi_r^2=1.09$ ) decay models. The inset shows a close-up of the initial interval of 600ps width and (d) shows the residues for the two models.

indicates fast ( $f$ ), intermediate ( $i$ ) and slow ( $s$ ) temporal components,  $\tau_k$  is the fluorescence emission lifetime ( $\tau_f < \tau_i < \tau_s$ ) and  $\text{erf}(z) = \frac{2}{\sqrt{\pi}} \int_0^z \exp(-\xi^2) d\xi$  is the error function. Eq.(1) takes the periodic train of excitation pulses and response time jitter of the SPAD into account, such that our data in Fig.1 do not require deconvolution processing.

Analysis of the OGB-1 fluorescence reveals the best agreement with a triple exponential decay approximation. The data are modeled using the function  $A_f I_f + A_i I_i + (1 - A_f - A_i) I_s$  with the fast  $I_f(t)$ , intermediate  $I_i(t)$  and slow  $I_s(t)$  decaying components (1) of normalized partial intensities  $A_f$ ,  $A_i$  and  $A_s = 1 - A_f - A_i$ , respectively. Fig.1(c) details a comparison between the double-exponential (olive curve) and triple-exponential (green curve) models applied to fluorescence from a 38 nM  $\text{Ca}^{2+}$  concentration sample (red points and curve). In both cases, the residues [Fig.1(d)] do not show any bias that might be caused by the Gaussian curve approximation of the IRF, while the quality of the numerical fit is improved in case of the triple-exponential model, as also

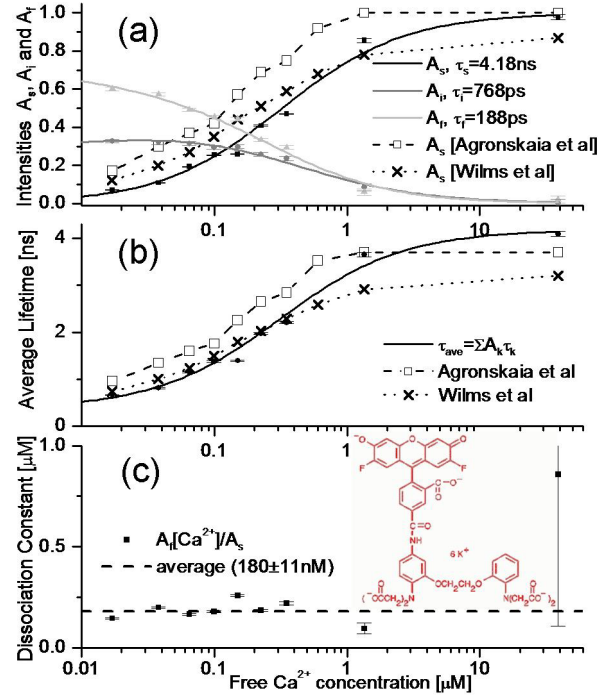


Fig. 2. (Color online) Partial intensities  $A_s$ ,  $A_i$  and  $A_f$  of the slow ( $\tau_s=4.18\pm 0.01\text{ns}$ ), intermediate ( $\tau_i=768\pm 16\text{ps}$ ) and fast ( $\tau_f=188\pm 6\text{ps}$ ) decay components (a) and the mean lifetime  $\tau_{\text{ave}} = \sum_k A_k \tau_k$  (b) of OGB-1 fluorescence as a function of the free  $\text{Ca}^{2+}$  concentration in comparison with the data from [4] and [5],  $\chi_r^2=0.96$ . The numerical fit to the model (2) (curves) yields  $K_D=195\pm 9\text{ nM}$ ,  $K_{Dn}=4\pm 6\ \mu\text{M}$  and  $n=9\pm 3$ . (c): The ratio  $A_f[\text{Ca}^{2+}]/A_s$  (points) and its variance-weighted mean yielding  $K_D=180\pm 11\text{ nM}$  (dashed line). The inset shows the structure of OGB-1 molecule.

confirmed by the reduced  $\chi^2$ -values. Wilms et al [5] have made the same observation for OGB-1 fluorescence in the absence of  $\text{Ca}^{2+}$ . However, it was attributed to contaminating dye derivatives and a double-exponential model has been utilized for samples containing  $\text{Ca}^{2+}$ . Previously reported data [1, 4, 5] for OGB-1 fluorescence lifetimes thus assume double-exponential decay. We argue that at high  $\text{Ca}^{2+}$  concentration, large amplitude of long-leaving component make it difficult to detect short lifetime components with small amplitudes and the FLIM systems used in [1, 4, 5] exhibit insufficient temporal resolution to enable observation of the triple-exponential behavior.

Using triple-exponential fluorescence decay (1) with the lifetimes independent of the calcium buffer [1, 5], we applied a global numerical analysis to our data, yielding the partial intensities  $A_k$  in function of free  $\text{Ca}^{2+}$  concentration and the lifetimes  $\tau_k$  (Fig.2). Temporal resolution of our system allows the short lifetime component ( $\tau_f \sim 188\pm 6\text{ps}$ ) to be unambiguously resolved in the background of the intermediate- and long-living fluorescence ( $\tau_i \sim 768\pm 16\text{ps}$  and  $\tau_s \sim 4.18\pm 0.01\text{ns}$ ). The partial intensities  $A_f$  and  $A_i$  decrease while the slow-component intensity  $A_s = 1 - A_f - A_i$  increases with concentration  $[\text{Ca}^{2+}]$ .

We attribute, as usual, the short- and long-lifetime components to, respectively, unbound and  $\text{Ca}^{2+}$ -bound OGB-1 with a simple 1:1 complex stoichiometry. As such and because the intensities are defined by complex concentrations, we obtain that  $A_f \propto [\text{D}]$  and  $A_s \propto [\text{CaD}] = K_D^{-1} [\text{Ca}^{2+}][\text{D}]$  with  $[\text{D}]$  and  $[\text{CaD}]$  being the unbound and Ca-bound OGB-1 concentrations and  $K_D$  the dissociation constant of the 1:1 complex. The ratio  $A_f[\text{Ca}^{2+}]/A_s$  thus yields an estimate of the dissociation constant. In Fig. 2 (c), a weighted average ratio  $180 \pm 11 \text{ nM}$  is in good agreement with the quoted (by manufacturer)  $K_D$  of 170 nM.

In Fig.2, the long lifetime component  $A_s$  is in good agreement with the measurements of Agronskaia *et al* [4] and Wilms *et al* [5], but in [5],  $A_s < 1$  in  $\text{Ca}^{2+}$ -saturated buffer and  $K_D$  is too high ( $\sim 300 \text{ nM}$ ). These discrepancies are attributed to the dye impurities and to the difference in two-photon absorption cross-sections of Ca-bound and unbound OGB-1, which are said difficult to be quantified [5].

For the Ca-bound OGB-1, Lakowicz [1] reported  $\tau_s$  of 4 ns, which agrees well with our data. In [4],  $\tau_s$  varies in the range 2.6-3.7 ns, while in [5],  $\tau_s = 3.63 \text{ ns}$ . For the Ca-free OGB-1, a single lifetime component  $\tau_f$  has been measured of 700 [1], 290-420 [4] and 346 ps [5], respectively. These results correspond to the combined effect of the decay processes with the lifetimes  $\tau_f \sim 190 \text{ ps}$  and  $\tau_i \sim 770 \text{ ps}$  in our measurements, which may not have been resolved in previous studies. The experimental setup in [5] relies on a commercially available Photomultiplier Tube (PMT) with a quoted timing jitter of 200 ps. Other data [1, 4] are reported without timing resolution of experimental setups.

Due to the Ca-binding features of the octadentate chelator BAPTA [9], the 1:1 stoichiometry is usually attributed to the Ca-bound OGB-1 as well. However, the molecule of OGB-1 has an asymmetric structure with respect to its BAPTA moiety (Fig.2, inset). The asymmetric arrangement of the carboxyl functional groups, benzol rings, fluorine and nitrogen atoms as well as the variations of electronic density from low (at hydrogen in carboxyl groups) to high (at benzol rings, F and O atoms) assume a polarity of the molecule and, as a consequence, weak dipole-dipole intermolecular forces. As a result of such interaction forces, several OGB-1 molecules might be coordinated to a Ca-bound OGB-1 forming thus a polymolecular association with a calcium:indicator molar ratio 1:n. The intermediate lifetime component  $\tau_i$  in Fig. 2 then might be attributed to such polymolecular association, yielding  $A_i \propto [\text{Ca}_{1/n}\text{D}] = K_{Dn}^{-1/n} [\text{D}][\text{Ca}^{2+}]^{1/n}$  with  $K_{Dn}$  being the corresponding dissociation constant. Note that formation of a polymolecular structure is a very complex processes and requires thorough investigations but a non 1:1 stoichiometry of Ca:OGB-1 has been reported in [10] and here it allows us to build an accurate model:

$$\frac{[\text{Ca}^{2+}]}{K_D} = \frac{A_s}{A_f} = \frac{A_s}{1-A_s} \left[ 1 + \frac{A_i}{A_f} \right], \quad \frac{[\text{Ca}^{2+}]}{K_{Dn}} = \left( \frac{A_i}{A_f} \right)^n. \quad (2)$$

In the limit  $K_{Dn} \rightarrow \infty$  (double exponential decay), it agrees with the Hill equation, as opposed to the model in [5]. The numerical fit of data in Fig.2 reports small binding affinity ( $K_{Dn} \sim 4 \mu\text{M}$ ) and  $n=9$  indicating the most probable form of

polymolecular association with eight Ca-free molecules coordinated to the Ca-bound OGB-1. The dissociation constant  $K_D$  reported by the fit is 195 nM, in agreement with the average of  $A_f[\text{Ca}^{2+}]/A_s$  (bottom panel).

The triple exponential fluorescence decay in non-ratiometric Ca probes as a result of dye contaminations was suggested by Lakowicz *et al* [11] for the Calcium Green (CG-1). The CG-1 molecule has the same structure as OGB-1 but the two F atoms are replaced by Cl, yielding [11]  $\tau_f = 50 \text{ ps}$ ,  $\tau_i = 450 \text{ ps}$  and  $\tau_s = 3.7 \text{ ns}$ . Interestingly, the signature of non-1:1 stoichiometry has been noticed for Ca-bound CG as well [12]. We find that at low  $\text{Ca}^{2+}$  concentration, the ratio  $A_f[\text{Ca}^{2+}]/A_s$  in [11] is a constant of  $170 \pm 20 \text{ nM}$ , yielding  $K_D$  close to the quoted value of 190 nM. At high Ca concentration, the band pass of the system (2GHz modulation using a frequency-domain FLIM technique) was insufficient to accurately measure the small component  $A_f$ . The data in [11] can thus be accurately interpreted in the framework of our model (2), without appealing to dye impurities. ( $K_D$  obtained in [11] using a conventional model [13] is 128nM).

In summary, we have shown that high-temporal resolution measurements of the triple-exponential fluorescence decay of non-ratiometric  $\text{Ca}^{2+}$  indicators allow the free  $\text{Ca}^{2+}$  concentration and dye dissociation constant to be measured precisely.

DLB is grateful to Leonid Zekel and Edwin Constable for discussions on the model. This research was supported, in part, by a grant of the Swiss National Science Foundation and by Centre SI of EPFL.

## References

1. J. Lakowicz, *Principles of Fluorescence Spectroscopy*, Plenum, New York (1999)
2. K. Suhling, P.M.W French and D. Phillips, *Photochem. Photo-biol. Sci.* **4**, 13(2005)
3. S. Cova, A. Longoni, A. Andreoni and R. Cubeddu, *IEEE J. Quantum Electron.* **19**, 630(1983)
4. A.V. Agronskaia, L. Tertoolen and H.C. Gerritsen, *J. Biomed. Opt.* **9**, 1230(2004)
5. C.D. Wilms, H. Schmidt and J. Eilers, *Cell Calcium* **40**, 73(2006)
6. C. Niclass, A. Rochas, P.A. Besse, and E. Charbon, *IEEE J. Solid-State Circuits* **40** 1847(2005).
7. W. Denk, J.H. Strickler and W.W. Webb, *Science* **248**, 73(1990)
8. A. Habenicht, J. Hjelm, E. Mukhtar, F. Bergstrom and L.B.A. Johansson, *Chem. Phys. Lett.* **354**, 367(2002)
9. R. Y. Tsien, *Biochemistry* **19**, 2396 (1980)
10. D. Thomas, S.C. Tovey, T.J. Collins, M.D. Bootman, M. J. Berridge, P. Lipp, *Cell Calcium* **28**, 213 (2000)
11. J. R. Lakowicz, H. Szmacinski, and M.L. Johnson, *J. of Fluorescence* **2**, 47 (1992)
12. M. Eberhard and P. Erne, *Biochem. and Biophys. Res. Comm.* **180**, 209 (1991)
13. G. Grynkiewicz, M. Poenie, and R. Y. Tsien, *J. Biol. Chem.* **260**, 3440 (1985)